Chemical Interaction and Enhanced Interfacial Ion Transport in Ceramic Nanofiber-Polymer Composite Electrolyte for All-Solid-State Lithium Metal Battery

Journal:	*Journal of Materials Chemistry A*
Manuscript ID	TA-ART-11-2019-012495.R1
Article Type:	Paper
Date Submitted by the Author:	22-Jan-2020
Complete List of Authors:	Yang, Hui; West Virginia University Bright, Joeseph; West Virginia University, Department of Mechanical and Aerospace Engineering Chen, Banghao; Florida Stat University Zheng, Peng; West Virginia University Gao, Xuefei; West Virginia University, Department of Mechanical and Aerospace Engineering Liu, Botong; West Virginia University, Department of Mechanical and Aerospace Engineering Kasani, Sujan; West Virginia University College of Engineering and Mineral Resources, Lane Department of Computer Science and Electrical Engineering Zhang, Xiangwu; North Carolina State University, Fiber and Polymer Science Wu, Nianqiang; West Virginia University,

Chemical Interaction and Enhanced Interfacial Ion Transport in Ceramic Nanofiber-Polymer Composite Electrolyte for All-Solid-State Lithium Metal Battery

Hui Yang[1], Joeseph Bright[1], Banghao Chen[2], Peng Zheng[1], Xuefei Gao[1], Botong Liu[1], Sujan Kasani[1],

Xiangwu Zhang[3], and Nianqiang Wu[1,4,,#]*

[1]Department of Mechanical and Aerospace Engineering, West Virginia University, Morgantown, WV 26506-6106, United States

[2]Chem & BioChem Department, Florida State University, Tallahassee, Florida, 32306, USA

[3]Fiber and Polymer Science Program, Department of Textile Engineering, Chemistry and Science, Wilson College of Textiles, North Carolina State University, Raleigh, NC 27695-8301, United States

[4]C. Eugene Bennett Department of Chemistry, West Virginia University, Morgantown, WV 26506-6045, USA

*To whom the correspondence should be addressed. Tel: +1-413-545-6175, E-mail: nianqiangwu@umass.edu

[#]*Current address: Department of Chemical Engineering, University of Massachusetts Amherst, Amherst, MA 01003-9303, United States*

ABSTRACT

This paper has reported the synergy between the ceramic nanofibers and the polymer, and the enhanced interfacial Li-ion transport along the nanofiber/polymer interface in a solid-state ceramic/polymer composite electrolyte, at which three-dimensional (3D) electrospun aluminum-doped $Li_{0.33}La_{0.557}TiO_3$ (LLTO) nanofiber network is embedded in polyvinylidiene fluoride-hexafluoropropylene (PVDF-HFP) matrix. Strong chemical interaction occurs between the nanofibers and the polymer matrix. Addition of the ceramic nanofibers into the polymer matrix results in the dehydrofluorination of PVDF chains, deprotonation of the $-CH_2$ moiety and amorphization of the polymer matrix. Solid-state nuclear magnetic resonance (NMR) spectra reveal that lithium ions transport via three pathways: (i) intra-polymer transport, (ii) intra-nanofiber transport, and (iii) interfacial polymer/nanofiber transport. In addition, lithium phosphate has been coated on the LLTO nanofiber surface before the nanofibers are embedded into the polymer matrix. The presence of lithium phosphate at the LLTO/polymer interface further enhances the chemical interaction between the nanofibers and the polymer, which promotes the lithium ion transport along the polymer/nanofiber interface. This in turn improves the ionic conductivity and electrochemical cyclic stability of the nanofiber/polymer composite. As a result, the flexible LLTO/Li_3PO_4/polymer composite electrolyte membrane exhibits ionic conductivity of 5.1×10^{-4} S/cm at room temperature and an electrochemical stability window of 5.0 V vs. Li/Li^+. The symmetric Li|electrolyte|Li half-cell shows a low overpotential of 50 mV at a constant current density of 0.5 mA/cm^2 for more than 800 h. In addition, a full cell is constructed by sandwiching the composite electrolyte between a lithium metal anode and a $LiFePO_4$-based cathode. Such an all-solid-state lithium metal battery exhibits excellent cycling performance and rate capability.

KEYWORDS: Solid-state electrolyte; ceramic-polymer composite; ion transport; lithium battery; interface

INTRODUCTION

Currently commercial lithium-ion batteries use liquid electrolytes that contain flammable substrates. This raises a concern on operational safety. Use of solid-state electrolytes is an alternative solution to flammable liquid electrolytes, which improves the chemical and thermal stability of Li-ion batteries. Researchers have been developing different types of solid-state electrolytes including ceramics, polymers, and ceramic-polymer composites. Ceramic electrolytes have much higher ionic conductivity than polymers. However, it is difficult to integrate ceramic electrolytes with electrodes due to large contact interfacial resistances.[1,2] In addition, the stability of ceramic electrolytes such as $Li_{0.33}La_{0.557}TiO_3$ (LLTO) is still of concern[3]. Dendrites can be formed at the Li metal electrode/electrolyte interface in ceramic electrolyte-based batteries if there is poor contact and/or exist defects in the ceramic electrolytes.[4,5] In contrast, polymer electrolytes are convenient for machining and integration with electrodes. However, current polymer electrolytes show poor ionic conductivity.[6-8] For example, the lithium salt-stuffed polyethyleneoxide (PEO) exhibits ionic conductivity on the order of 10^{-6}-10^{-9} S/cm at room temperature.[9,10] To utilize the merits of both ceramic and polymers and to compensate their shortcomings, inorganic fillers are incorporated into polymers to form solid-state ceramic-polymer composite electrolytes. These inorganic fillers not only enhance the ionic conductivity, but are also beneficial to integration of electrolytes with electrodes. It has been reported that inorganic spherical particles including active lithium ion conductors (Li_3N_{16}[11]), LLTO[12] and inactive fillers (Al_2O_3[13] and SiO_2[14]) have been added into the polymers, which increases mechanical strength, suppresses crystallization of polymer matrix, and improves ionic conductivity and cyclic stability. However, agglomeration of particles usually happens in the ceramic-polymer composites when a large content of inorganic particles are added into polymer matrix. Particle agglomeration leads to non-uniform presence of large amount of crystallized polymer in different regions of the electrolyte[15, 16]. In contrast, long ceramic nanofibers can form a three-dimensional (3D) uniform network within the polymer matrix in the nanofiber-polymer composite, eliminating the particle agglomeration problem.

The 3D inorganic nanofiber network not only improves the mechanical strength of the electrolyte membrane, but also provides continuous ion transport channels through the inter-woven inorganic nanofibers or along the nanofiber/polymer interface. Therefore, solid-state inorganic nanofiber-polymer composite electrolytes have aroused considerable research interest[17-20].

So far the ionic conductivity (10^{-5} ~10^{-4} S/cm) of the state-of-the-art solid-state inorganic nanofiber-polymer composite electrolytes are two orders of magnitude lower than that (1×10^{-2} S/cm) of conventional liquid electrolytes used in commercial lithium-ion batteries. To improve their ionic conductivity, extensive study has been focused on enhancing the ionic conductivity of both ceramic fillers and polymer matrix. Few studies have focused on the interface between ceramic fillers and polymer matrix.[21-25] The ceramic/polymer interface needs to be engineered to enable the interaction and synergy between ceramic and polymers. On the other hand, the chemical interaction of polymer with ceramic remains poorly characterized. In addition, the lithium ion transport pathway in the ceramic-polymer composite electrolytes needs to understood.

To address the issues above, a solid-state ceramic nanofiber-polymer composite electrolyte is developed, in which a lithium phosphate (Li_3PO_4) modified three-dimensional (3D) LLTO nanofiber network is embedded into a polyvinylidiene fluoride-hexafluoropropylene (PVDF-HFP) polymer matrix. PVDF-HFP is chosen as the composite matrix because it has higher Li-ion conductivity than PEO. PVDF-HFP has relatively lower crystallinity due to the copolymerization effect between VDF and HFP in comparison with poly(vinylidene fluoride) (PVDF). To enhance the ionic conductivity of the pervoskite-type LLTO nanofibers, Al is doped into LLTO with different concentrations ($Li_{0.33}La_{0.557}Ti_{1-x}Al_xO_3$ (LLATO), x=0.005, 0.01, 0.015, 0.05, 0.1 are named as LLATO, LLATO-1, LLATO-2, LLATO-3, LLATO-4, respectively). In addition, a layer of Li_3PO_4 is coated on the surface of LLATO nanofibers to enhance the chemical interaction between nanofibers and polymer and to improve the ionic conductivity of composite electrolyte. This study also aims to gain fundamental understanding of the interfacial interaction and Li ion transport pathways. Microscopic and spectroscopic techniques such as Raman, Fourier transform infrared (FTIR), X-ray photoelectron spectroscopy (XPS) and solid-state nuclear magnetic resonance (NMR) are combined with electrochemical analysis to characterize the interfacial chemical interaction between the LLATO nanofibers and the polymer matrix. Solid-state ^{6}Li NMR and electrochemical impedance spectroscopy (EIS) are used to investigate the Li-ion transport pathways in the nanofiber-polymer composite and to elucidate the role of Li_3PO_4 in Li-ion transport. Furthermore, lithium dendrite formation is examined after repeated discharging and charging.

RESULTS

Morphology and microstructure of LLATO nanofibers LLTO nanofibers were prepared by electrospinning. Figure S1 shows the scanning electron microscope (SEM) images of LLTO nanofibers calcined at different temperatures. "Inter-welded" nanofibers were obtained at 900°C, which was the optimized temperature. LLTO nanofibers were then doped with different contents of aluminum with a nominal range of 0.5~10 mol%. It is believed that Ti^{4+} substitution by Al^{3+} changes the bond strength between the B-site cation and oxygen, thus enhances the ionic conductivity of the LLTO nanofibers.[26] As shown in Figure 1a, the as-spun precursor nanofibers, which were composed of polyvinylpyrrolidone (PVP) and salts, possessed a smooth surface with an average diameter of about 184 nm. The PVP polymer in the precursor fibers was eliminated after calcination at 900 °C. The diameter of the obtained LLATO nanofibers was reduced to 155 nm, showing a roughened surface. The LLATO nanofibers were "inter-welded" with each other, forming a cross-linked 3D nanofiber networks (Figure 1b). Figure 1d and Figure 1e show the corresponding diameter distribution; and Figure S2 reveals the SEM images of 1-10% aluminum-doped LLTO. Figure 1c displays the TEM image of a single LLATO nanofiber, indicating its polycrystalline structure composed of small interconnected grains.

A thin layer of Li_3PO_4 was coated on the surface of the LLATO nanofibers by immersing LLATO nanofibers into a Li_3PO_4 solution. The thin Li_3PO_4 coating increased the lithium ion concentration on the nanofiber surface, and enhanced the wettability between the LLATO nanofibers and the polymer.

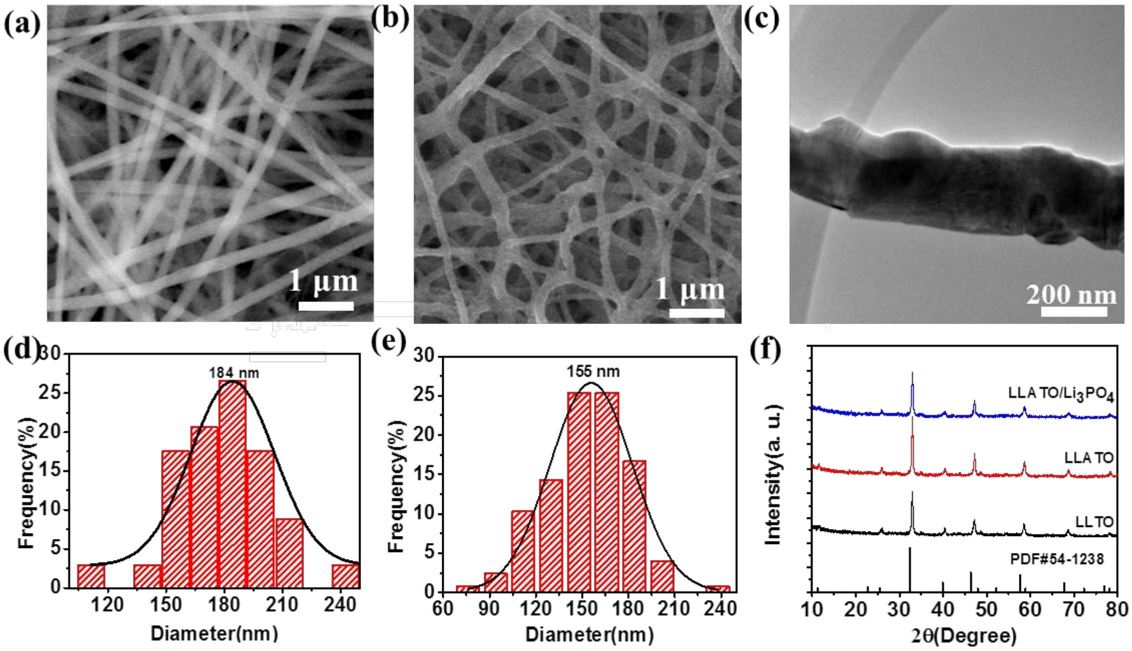

Figure 1. (a) SEM image of as-spun PVP precursor nanofibers of LLATO, (b) LLATO nanofibers after calcination at 900 °C, (c) TEM image of LLATO nanofibers, (d) diameter distribution of as-spun PVP precursor nanofibers, (e) diameter distribution of LLATO nanofibers after calcination at 900 °C, (f) XRD patterns of LLTO and LLATO nanofibers.

Powder X-ray diffraction (XRD) patterns were taken at room temperature to characterize the crystal structure of the nanofibers. After calcination of the as-spun nanofibers at 900 °C in air, all the LLATO nanofibers (LLATO-1 to LLATO-4 in Figure S3) exhibited perovskite-type structure according to the Joint Committee on Powder Diffraction Standard (JCPDS) card 54-1238, as shown in Figure 1f, confirming the tetragonal crystalline structure of materials. The XRD spectra for the 1.5%, 5%, 10% Al-doped LLTO showed the reduced intensity and slight shift as compared to pristine LLTO. This was due to the lattice distortion and the reduced crystallinity by the insertion of Al^{3+} ions into the LLTO nanofibers. After surface-modification with Li_3PO_4, the surface of LLATO nanofibers became rougher (Figure S4a). FT-IR spectra were also used to confirm the coating of Li_3PO_4. The absorption band at 1055 cm^{-1} in Figure S4b was attributed to the asymmetric stretching (v3) vibration mode of isolated tetrahedral PO_4 units.[28-29] XPS was further carried out to confirm the coating of Li_3PO_4 on the surface. The P 2p peak appeared at 133.8 eV in the XPS spectra (Figure S5), which was due to the presence of Li_3PO_4, indicating successful coating of Li_3PO_4 onto the nanofiber surface. However, the XRD pattern of LLTO nanofibers did not change after coating of Li_3PO_4 (Figure 1f).

Microstructure of composite electrolyte An acetone solution containing PVDF-HFP and lithium bis(trifluoromethanesulfonyl)imide (LiTFSI) was directly dropped to the calcinated nanofiber membrane, and dried to form composite electrolytes with 10-30 wt% of LLATO nanofibers. Taking the composite electrolyte with 30 wt% LLATO nanofibers as an example (Figure 2). The surface of composite was smooth and all voids of the nanofiber network were completely filled with the PVDF-HFP/LiTFSI polymer (Figure 2b, Figure S6-S7). The cross-section image of the electrolyte shows that it was about ~80 μm thick (Figure 2c). If the LLATO content exceeded 40 wt%, the void space of the porous nanofiber network cannot be completely filled by the polymer, which will cause the composite electrolyte to crack easily when assembling lithium cells. In addition, lithium dendrites will penetrate the porous structure of the nanofiber network (Figure S8).

Figure 2d reveals a high-resolution transmission electron microscope (HRTEM) image of bare LLATO nanofiber, which demonstrated high crystallinity within each grain with an inter-planar spacing of 0.20 nm, corresponding to the (004) plane of LLATO. Coating with Li_3PO_4 resulted in the formation of a LLATO/Li_3PO_4 core/shell structure (Figure 2e and 2f). A coating with a full surface coverage can the seen in Figure 2e, and the observed interplanar distance from Figure 2f of the outer coating of the nanofibers is 0.30 nm, corresponding to the (200) plane of Li_3PO_4. Special attention was paid to the interface between the inorganic nanofiber and the polymer. A clear and sharp boundary was observed between the uncoated nanofiber and polymer in the PVDF-HFP/LiTFSI/LLATO composite electrolyte (Figure 2g); and PVDF-HFP appeared amorphous while LLATO still retained its crystallinity. In contrast, the boundary between the Li_3PO_4-coated nanofiber and polymer in the PVDF-HFP/LiTFSI/LLATO/Li_3PO_4 composite electrolyte was no longer sharp and distinct (Figure 2h). There was still a thin layer of Li_3PO_4 attached on the surface of the LLATO nanofibers. However, Li_3PO_4 was found to penetrate into the amorphous PVDF-HFP polymer matrix, showing a gradient distribution of Li_3PO_4 from the nanofiber surface to the polymer matrix.

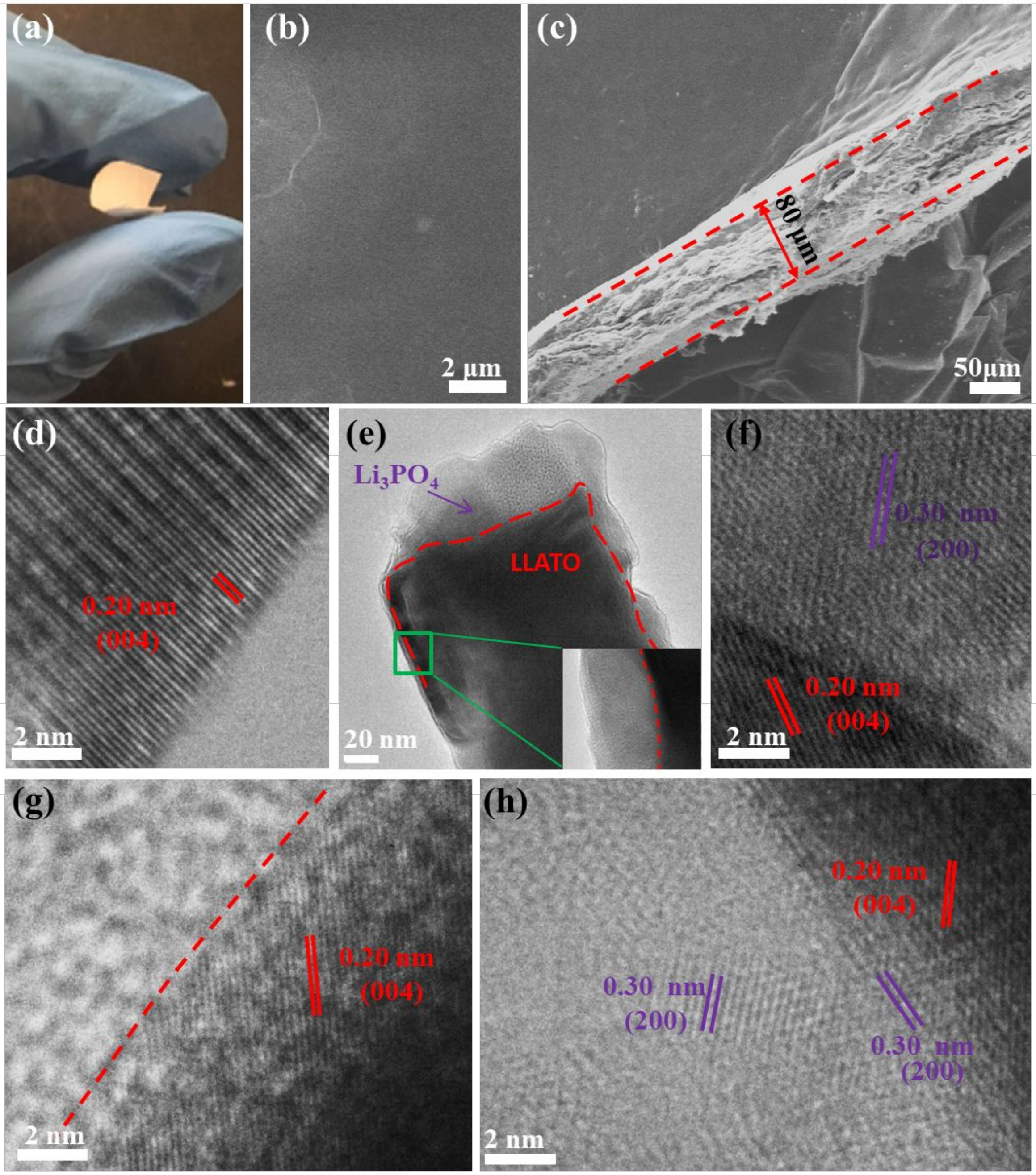

Figure 2. (a) Photograph of the flexible and bendable PVDF-HFP/LiTFSI/LLATO membrane, (b) SEM image of the surface of PVDF-HFP/LiTFSI/LLATO membrane, (c) cross-sectional SEM image of PVDF-HFP/LiTFSI/LLATO membrane, (d) TEM image of LLATO nanofibers, (e) TEM, inset is zoomed view of the marked box region, (f) HRTEM image of Li_3PO_4 LLATO nanofibers, (g) interface of PVDF-HFP/LiTFSI/LLATO composite electrolyte, (h) interface of PVDF-HFP/LiTFSI/LLATO/Li_3PO_4 composite electrolyte.

Ionic conductivity of composite electrolyte The ionic conductivity of the composite electrolyte was characterized with electrochemical impedance spectroscopy (EIS). EIS measurement was performed on the composite electrolyte sandwiched between two stainless-steel blocking electrodes in the frequency range from 1 Hz to 1MHz. Figure S9 shows the typical Nyquist plots of the composite electrolytes based on LLATO nanofibers with different contents of aluminum doping. The real axis intercept at a high frequency region was ascribed to the relaxation behavior in the bulk of composite electrolyte. There was one well-defined semicircle in the intermediate frequency region, indicating no electrode reaction at the electrode/electrolyte interfaces. The inclined straight tail in the low frequency region was due to the migration of lithium lions and the surface in-homogeneity of the electrodes.[30] The ionic conductivity was calculated by the formula[19]:

$$\sigma = \frac{L}{RA} \tag{1}$$

where L is the thickness of the composite electrolyte membrane, R is the resistance, and A is the effective electrode area. Without aluminum doping, PVDF-HFP/LiTFSI/LLTO exhibited ionic conductivity of 2.1 × 10^{-4} S/cm at room temperature. With 0.5% aluminum doping ($Li_{0.33}La_{0.557}Ti_{1-x}Al_xO_3$ (LLATO), x=0.005) in ceramic nanofibers, PVDF-HFP/LiTFSI/LLATO showed much higher ionic conductivities of 4.0 × 10^{-4} S/cm. Gradually decrease in ionic conductivity was observed with more aluminum doping (3.6 × 10^{-4} , 1.9 × 10^{-4}, 1.1 × 10^{-4}, 0.8 × 10^{-4} S/cm with LLATO-1 (x=0.01), LLATO-2 (x=0.015), LLATO-3 (x=0.05), LLATO-4 (x=0.1), respectively). Figure 3a shows the Nyquist plots of the PVDF-HFP/LiTFSI/LLATO composite electrolytes with 10-30 wt% LLATO. The ionic conductivity of PVDF-HFP/LiTFSI composite electrolyte with 10%, 20% and 30% contents of LLATO nanofibers were estimated to be 1.7×10^{-4} S/cm, 2.4×10^{-4} S/cm and 4.0×10^{-4} S/cm, respectively, at room temperature. The ionic conductivity of the PVDF-HFP/LiTFSI/30%LLATO was four times higher than that of the PVDF-HFP/LiTFSI electrolyte (1.1×10^{-4} S/cm). Obviosly the ionic conductivity of composite electrolyte increased with an increase in the cermaic filler content. Coating with Li_3PO_4

further increased the ionic conductivity, leading to 5.1×10^{-4} S/cm for the PVDF-HFP/LiTFSI/30%LLATO/Li_3PO_4 composite electrolyte.

Figure 3b shows the Arrhenius plot of the PVDF-HFP/LiTFSI/LLATO/Li_3PO_4 composite electrolytes. The relationship between ionic conductivity and temperature follows the traditional Arrhenius equation,

$$\sigma(\mathrm{T}) = \mathrm{a}\cdot\exp\left(-\frac{E_A}{RT}\right) \tag{2}$$

where a is the pre-exponential factor, E_A is the activation energy of the activated ion-hopping conduction process, and R is the universal gas constant (8.314 J mol^{-1}). Based on this equation, the activation energy obtained was 0.23 eV for the PVDF-HFP/LiTFSI/30%LLATO electrolyte, and 0.22 eV for the PVDF-HFP/LiTFSI/LLATO/Li_3PO_4 electrolyte (Table 1).

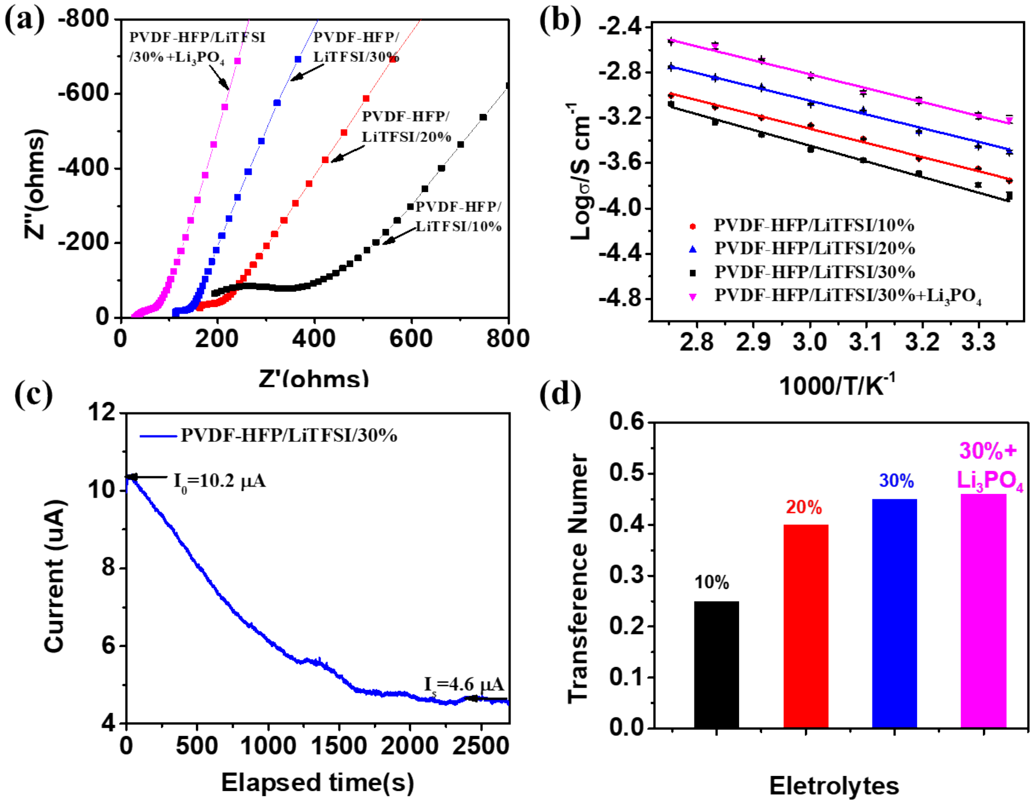

Figure 3. (a) EIS plots of composite electrolytes with different contents of LLATO nanofibers. (b) Arrhenius plots of the composite electrolytes. (c) Chronoamperometry profiles in Li/ PVDF-HFP/LiTFSI/LLATO /Li with a

step potential of 10 mV. (d) Lithium transference number of PVDF-HFP/LiTFSI/LLATO with different contents of LLATO nanofibers, and PVDF HFP/LiTFSI/LLATO/Li_3PO_4 sample.

Table 1. Ionic conductivity and activation energy of composite electrolytes with different contents of LLATO nanofibers.

Samples	Nanofiber amount (wt%)	Ionic Conductivity (S/cm) (at 25 ˚C)	Activation Energy (eV)
PVDF-HFP/LiTFSI/LLATO(10)	10	1.7×10^{-4}	0.28 ± 0.01
PVDF-HFP/LiTFSI/LLATO(20)	20	2.4×10^{-4}	0.25 ± 0.01
PVDF-HFP/LiTFSI/LLATO(30)	30	4.0×10^{-4}	0.23 ± 0.02
PVDF-HFP/LiTFSI/LLATO(30)/Li_3PO_4	30+Li_3PO_4	5.1×10^{-4}	0.22 ± 0.01

The lithium transference number of monolithic polymer was only 0.18 (Table S1), it increased as an increase in the content of nanofibers as shown in Figure 3c and 3d, and reached 0.45 when the nanofiber content was 30%. Generally anions in polymer move typically 5-10 times faster than Li ions. Increasing the lithium transference number helps reduction of the charge concentration gradient and the reversed cell polarization effect. Therefore, it can improve the cyclic stability of electrolyte. Moreover, the interaction among Li^+ ions, the partially dehydrofluorinated PVDF-HFP, and the LLATO nanofibers via acid-base interactions which will be discussed later, can help dissociate the LiTFSI salt, leading to an increase in the Li^+ carrier concentrtion.[17]

Electrochemical stability window and cycling performance of composite electrolyte It is essential to have a large electrochemical window for electrolytes in order to develop high-voltage lithium batteries. Liner sweep voltammetry (LSV) was obtained from the PVDF-HFP/LiTFSI/LLATO/Li_3PO_4 composite electrolyte using a stainless-steel plate as the working electrode, and a lithium foil as the counter electrode. Figure 4a shows the LSV profile of the PVDF-HFP/LiTFSI/LLATO/Li_3PO_4 composite electrolyte, demonstrating a stable voltage window up to 5 V vs. Li/Li^+.

The cyclic stability of the PVDF-HFP/LiTFSI, PVDF-HFP/LiTFSI/LLATO and PVDF-HFP/LiTFSI/LLATO/Li_3PO_4 electrolytes was evaluated with a symmetric Li|Electrolyte|Li cell. The composite electrolyte membrane was sandwiched between two lithium metal foils and sealed in coin cell in a glovebox. Figure S10 shows the thickness of the composite electrolytes. The symmetric cell was periodically charged and discharged at a constant current density of 0.5 mA/cm^2 for 0.5 h at room temperature to mimic the operation of charging and discharging process of lithium metal batteries. Figure 4b,4d and 4f shows the time-dependent voltage profiles. At room temperature, the Li|PVDF-HFP/LiTFSI|Li cell showed a polarization voltage of ~1 V due to the poor ionic conductivity of the electrolyte (Figure 4b), and short-circuiting happened after only 25 cycles. The reversible cycling performance of the Li|PVDF-HFP/LiTFSI/LLATO|Li cell was greatly improved, and it was stable for 600 h, showing a polarization voltage of 100 mV (Figure. 4d). The Li|PVDF-HFP/LiTFSI/LLATO/Li_3PO_4|Li cell exhibited a polarization voltage as low as 44 mV before 150 hours (Figure 4f). And the over-potential decreased to 34 mV after 150 hours of the charging/discharging process, which could be ascribed to the improved interface between the electrolyte membrane and lithium metal during the repeated Li electrodeposition.[20] (Figure 4f). The SEM images in Figure 4 show the morphology difference among the post-cycled samples. The presence of Li_3PO_4 at the ceramic/polymer interface in the composite electrolyte effectively suppressed the growth of interfacial products. As shown in Figures 4g, the surface morphology of the cycled PVDF-HFP/LiTFSI/LLATO/Li_3PO_4 composite electrolyte did not display obvious changes on the membrane surface. However, numerous round dots were visible on the membrane surfaces of the cycled PVDF-HFP/LiTFSI (Figure. 4c) and PVDF-HFP/LiTFSI/LLATO electrolyte membranes (Figure. 4e), indicating the interfacial product growth. [4]

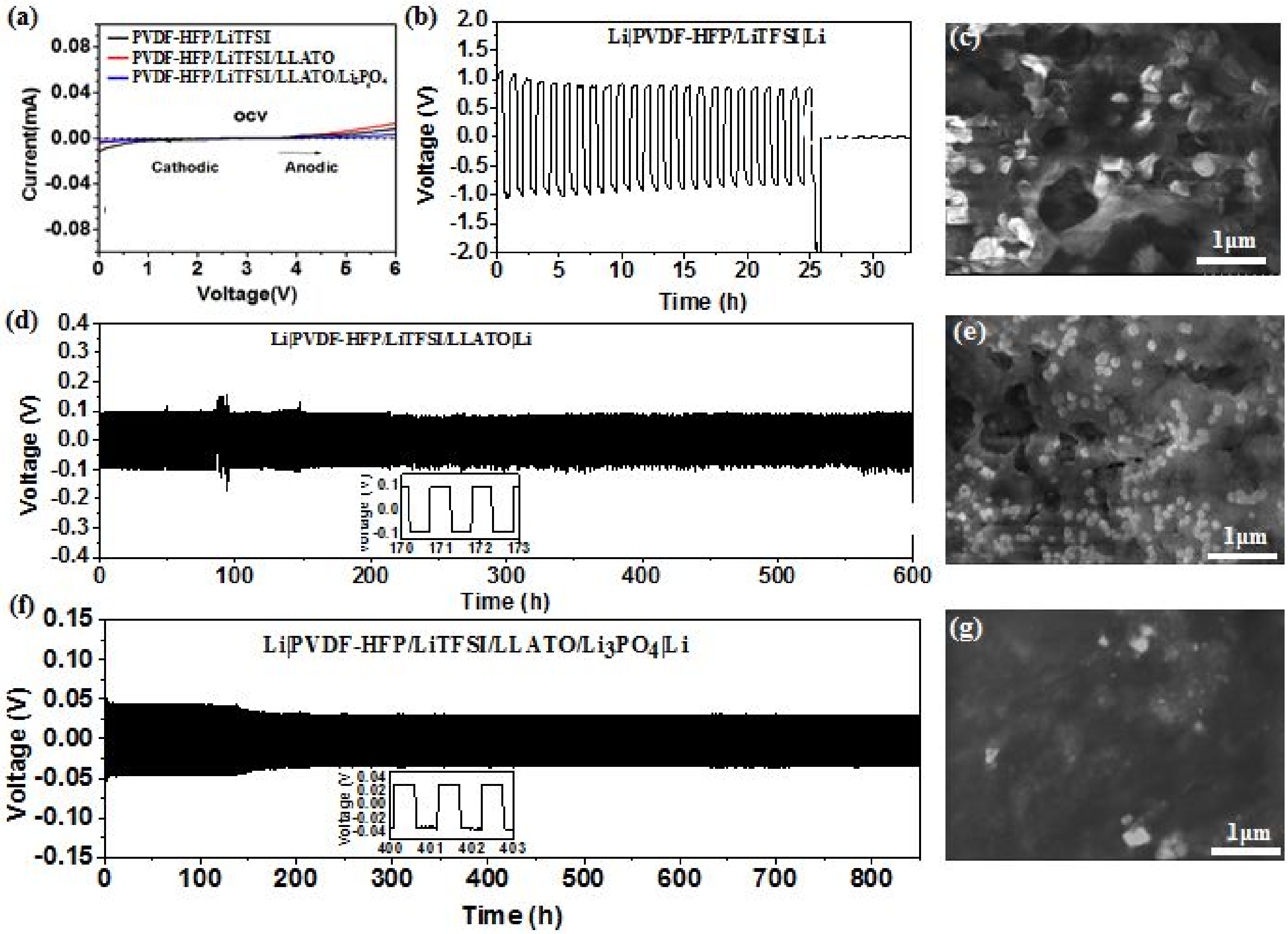

Figure 4. (a) LSV curve of composite electrolyte membrane to show the electrochemical stability window, Voltage profile at a current density of 0.5 mA/cm^2 for (b) Li|PVDF-HFP/LiTFSI|Li, (d) Li|PVDF-HFP/LiTFSI/LLATO |Li, and (f) Li|PVDF-HFP/LiTFSI/LLATO/Li$_3$PO$_4$|Li. Top view SEM images of composite electrolyte after charging/discharging cycling test for (c) Li|PVDF-HFP/LiTFSI|Li, (e) Li|PVDF-HFP/LiTFSI/LLATO|Li, and (g) Li|PVDF-HFP/LiTFSI/LLATO/Li$_3$PO$_4$|Li.

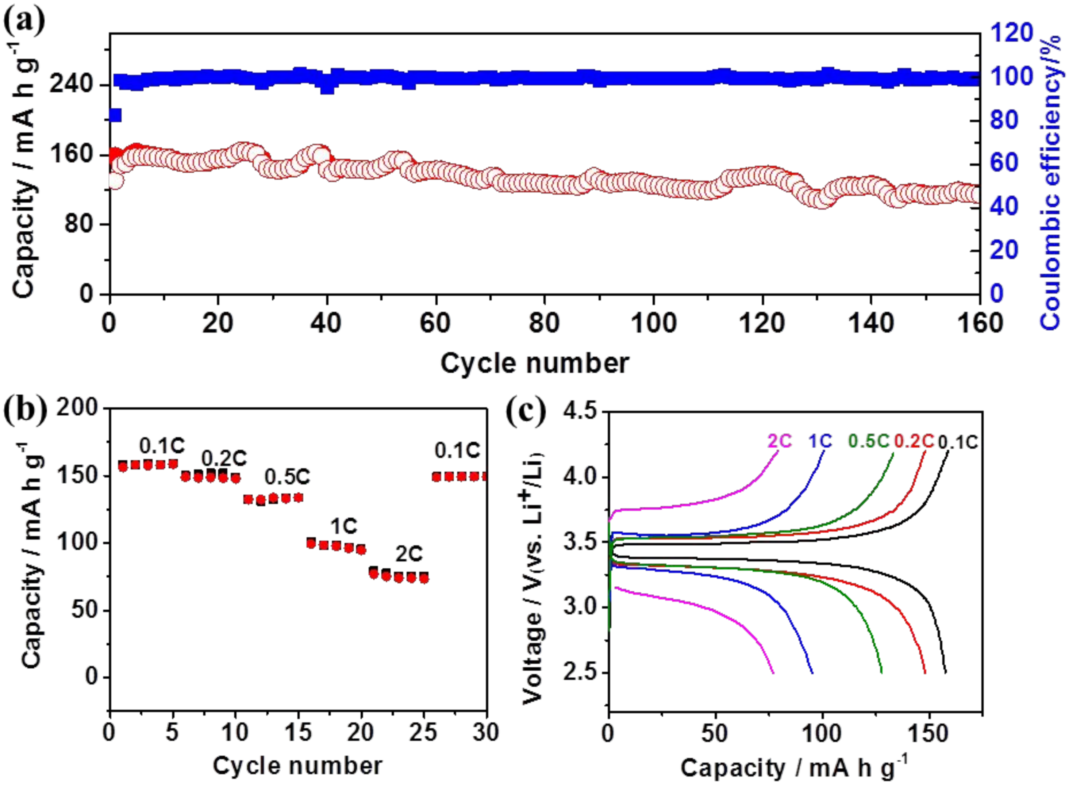

Figure 5. (a) Cycling performance of a Li|PVDF-HFP/LiTFSI/LLATO/Li_3PO_4|LFP coin cell at 0.5 C at 25 °C. (b) Rate capability at 0.1C, 0.2C, 0.5C, 1C and 2C. (c) Charge/discharge curves of the Li|PVDF-HFP/LiTFSI/LLATO/Li_3PO_4|LFP coin cell at various rates.

Full CR2032 coin cells were constructed for the lithium batteries with the PVDF-HFP/LiTFSI/LLATO/Li_3PO_4 composite membrane as the electrolyte, a Li metal foil as the anode and the $LiFePO_4$-based material as the cathode. The cycling performance of the full-cell battery was tested at a current rate of 0.5C and 1C (1C = 170 mA g^{-1}) at 25 °C between 2.5 and 4.2 V. Figure 5a shows the galvanostatic charging and discharging profiles. The cell delivered the specific discharge capacity of 130.7 mA h g^{-1} at a current rate of 0.5 C and retained 87.8% (114.7 mA h g^{-1}) of the initial capacity after 160 cycles. The Coulombic efficiency remained over 99.4% after 160 cycles. Furthermore, the full cell displayed excellent rate performance. The reason for fluctuation of the capacity of Li|PVDF-HFP/LiTFSI/LLATO/Li3PO_4|LFP coin cell was not clear to the best of our knowledge. One of possible reasons was that some cycles were perturbed by the change in material or in contact during testing. The capacity fading should be mainly due to the interface change between the electrolyte and the Li metal. The PVDF-HFP/LiTFSI/LLATO/Li_3PO_4 polymer/ceramic electrolyte may also change during testing. As shown in Figure 5b, the discharging capacity was measured to be 158, 147, 133, 98, and 76 $mAh·g^{-1}$ at rate of 0.1C, 0.2C, 0.5C, 1C and 2C, respectively. When the current rate was switched back to 0.1 C, the cell exhibited a reversible capacity of 149 mA h g^{-1}. As compared to the full cell with a commercial liquid electrolyte, the counterpart with the optimized PVDF-HFP/LiTFSI/LLATO/Li_3PO_4 electrolyte exhibited a longer cycling lifetime.[30,31] These results indicated that the PVDF-HFP/LiTFSI/LLATO/Li_3PO_4 composite was promising for use in lithium metal batteries.

DISCUSSION

Interaction between ceramic nanofibers and polymer matrix XRD patterns were acquired from PVDF-HFP, PVDF-HFP/LiTFSI, and composite electrolytes with different contents of LLATO at room temperature in order to characterize the crystalline phases of the composite electrolyte (Figure 6a). Pristine PVDF-HFP polymer membrane showed strong characteristic diffraction peaks in 2θ range of 18° and 20° with relatively weak peaks at around 27° and 40°, indicating a high degree of crystallinity. After the lithium salt (LiTFSI) was added into the polymer, the characteristic diffraction peaks of PVDF-HFP became weak. The crystallinity of PVDF-HFP in the composite electrolyte further decreased as the LLATO nanofiber contents increased from 10% to 30%. It is well known that amorphization of polymer matrix increases motion of polymer chain segments and mobility of lithium ions. This is important for the conductivity improvement in the PVDF-HFP/LiTFSI/LLATO composite electrolytes.

The chemical interaction between the inorganic nanofibers and polymer were further investigated with vibration spectroscopy and photoemission spectroscopy. After addition of the lithium salt (LiTFSI) and ceramic nanofibers, the vibration modes of the PVDF-HFP complex was altered in both the shape and intensity. The Raman peaks at 795 cm^{-1} and 1426 cm^{-1} were assigned to the CH$_2$ rocking vibration and CH$_2$ wagging modes of α phase PVDF-HFP, respectively. The Raman peak at 873 cm^{-1} was attributed to the C-C symmetric stretching (Figure 6b).[32] The intensity of the peaks at 795 cm^{-1}, 873 cm^{-1}, and 1426 cm^{-1} decreased after the adding the lithium salt LiTFSI and LLATO nanofibers to the PVDF-HFP matrix. The decreased Raman peak intensities indicate the deprotonation of -CH$_2$ moiety and a weakened α phase due to the introduction of LiTFSI. On the other hand, the CF$_2$ stretching vibration mode at 1200 cm^{-1} of PVDF-HFP also decreased dramatically. The decrease in the CF$_2$ stretching vibration was associated with interactions between lithium salt and CF$_2$ groups in the polymer molecular chains.[33] In the FTIR spectra (Figure 6c), the CH$_2$ bending vibration mode peak at 2980 cm^{-1} decreased dramatically after the addition of LLATO nanofibers, indicating deprotonation of CH$_2$ in PVDF-HFP.[17, 34] A new FTIR peak appeared at 1510 cm^{-1} after adding LLATO nanofibers to the composite, which was attributed to the C=C stretching vibration modes of polyenes, suggesting the dehydrofluorination of PVDF chains. These changes in the chemical structure were consistent with those of PVDF after alkaline treatment. Therefore, addition of LLATO was likely to create an alkaline-like condition for PVDF-HFP and caused a change in the chemical structure of PVDF-HFP.[33-35]

Figure 6e displays the XPS spectra of F 1s core-level from different samples. For the pristine PVDF-HFP polymer, the F 1s shows two sub-peaks with binding energy of 689.4 eV and 688.2 eV, which was ascribed to CF$_3$ and CF$_2$, respectively.[33] The binding energy of both peaks corresponding to CF$_3$ and CF$_2$ negatively shifted to 688.9 eV and 687.8 eV after the lithium salt LiTFSI was incorporated into the polymer, indicating partial reduction of F of PVDF-HFP. Due to the extraction of fluorine via the dehydrofluorination reaction after the addition of LLATO nanofibers, there was a new sub-peak attributed to the CF bond appeared in the C 1s spectra at binding energy of 287.6 eV, as shown in Figure S11-14. Adding Li$_3$PO$_4$ attenuated the strong polar effect of F on lithium ions as shown by the negative binding energy shift of CF$_3$ and CF$_2$ to 688.2 and 687.3 eV, respectively, as shown in Figure 6e.

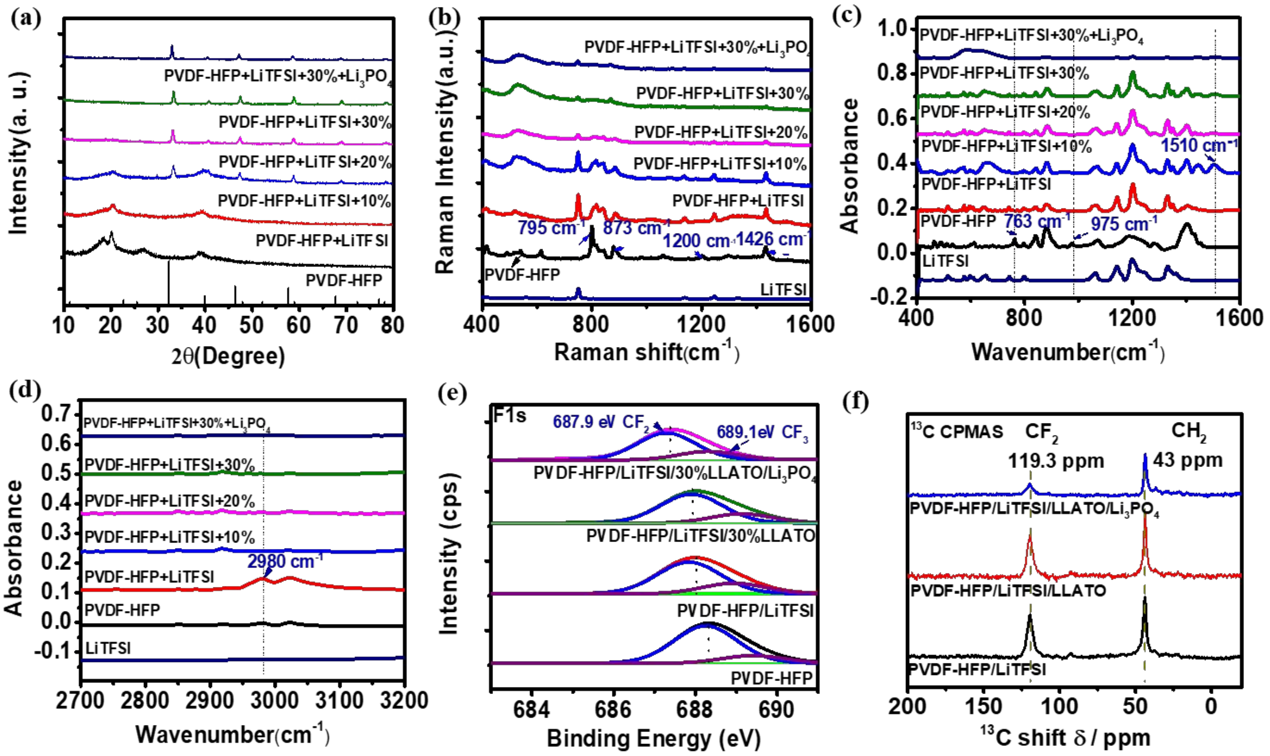

Figure 6. (a) XRD patterns, (b) Raman spectra, (c), (d) FTIR spectra, (e) XPS C1s core-level spectra, and (f) ^{13}C NMR spectra of pure PVDF-LiTFSI, PVDF-LiTFSI/LLATO, and PVDF-LiTFSI/LLATO-Li_3PO_4 nanofiber-based membranes.

The ^{13}C nucleus is very sensitive to its local electronic environment. As such, the polymer matrix structure was assessed by solid-state ^{13}C NMR, to understand how the polymer micro-structure was influenced by introduction of the inorganic nanofibers [36]. Figure 6f shows the solid-state ^{13}C NMR (and ^{13}C NMR in Figure S15) for PVDF-HFP/LiTFSI, PVDF-HFP/LiTFSI/LLATO and PVDF-HFP/LiTFSI/LLATO/Li_3PO_4. The two peaks at ~43.0 and ~120 ppm are attributed to the resonances of the –CH_2– and –CF_2– groups in PVDF-HFP, respectively [37.] The peaks of carbon atoms attached to the –CF_3 group of PVDF-HFP were too small to be seen in Figure 6f. The peaks of the carbons (–CF–) from HFP appeared at ~92 ppm. Note that the CH_2 and CF_2 signals were of similar intensity in PVDF-HFP/LiTFSI, which was in accordance with PVDF-HFP itself.[37, 38] However, the intensity ratio between the CF_2 and CH_2 signals decreased in the PVDF-HFP/LiTFSI/LLATO, and further decreased in the

PVDF-HFP/LiTFSI/LLATO/Li_3PO_4. This gave direct evidence of dehydrofluorination of PVDF chains, which was in agreement with the Raman and FTIR spectra results.

Lithium ion transport pathways The local environment and transport pathways of Li ions in the composite electrolyte was investigated by ^{6}Li and ^{7}Li NMR spectroscopy. Li-ions inside the polymer phase, the ceramic phase, and at the polymer–ceramic interface within composite electrolytes can be distinguished through the NMR test. ^{6}Li NMR was firstly used to characterize the composite electrolyte before the $^6Li\rightarrow^7Li$ isotope replacement as shown in Figure 7a. PVDF-HFP/LiTFSI, pure LLATO, and pure Li_3PO_4 were used as references in the analysis. The lithium salt (LiTFSI) in the PVDF-HFP/LiTFSI matrix exhibited the ^{6}Li NMR signal at -0.96 ppm. Pristine LLATO showed the ^{6}Li NMR peaks at -0.81, -0.25, 0.13, 1.8, and 2.4 ppm. Pristine Li_3PO_4 showed a sharp ^{6}Li NMR peak at 0.33 ppm, and shoulder at around 0 ppm. In the composite electrolyte such as PVDF-HFP/LiTFSI/LLATO and PVDF-HFP/LiTFSI/LLATO/Li_3PO_4, the ^{6}Li NMR signals of each components can be distinctively observed in Figure 7a. Because of the overlapping with Li_3PO_4 ^{6}Li NMR signals, the peak intensity attributed to LLATO is relatively weak compared with that of the LLATO and PVDF-HFP/LiTFSI/LLATO samples. At the same time, some peaks are broadened. In the curve of PVDF-HFP/LiTFSI/LLATO/Li_3PO_4 (as observed from Figure 7a and 7c), there is a weak ^{6}Li peak located at 2.44 ppm and -0.81 ppm, which is attributed to LLATO. The broaden peak from 0.6 ppm to -0.15 ppm is due to the overlap of ^{6}Li signals from Li_3PO_4 and LLATO.

The $^6Li\rightarrow^7Li$ isotope replacement was then realized through electrochemical cycling of a symmetric ^{6}Li|composite electrolyte|^{6}Li cell to determine the possible transport pathways of Li ions in the composite electrolyte.[39-41] The ^{6}Li ions replaced the ^{7}Li ions in the electrolyte when the ^{6}Li ions moved from one electrode to the other electrode during battery cycling with a trail of ^{6}Li left along the transport pathway. Figure 7b-7d shows the comparison of the composite electrolytes before and after $^6Li\rightarrow^7Li$ replacement. After $^6Li\rightarrow^7Li$ replacement, the ^{6}Li resonance at -0.17 were observed for LiTFSI within the PVDF-HFP polymer matrix as shown in Figure 7d. There was an obvious ^{6}Li resonance shift when compared with the sample before cycling, indicating the change in the Li-ion local environment. For PVDF-HFP/LiTFSI/LLATO, the ^{6}Li peaks of LLATO at -0.30 and 0.13ppm shifted to -0.33 ppm and 0.19 ppm, respectively, with the peak intensities increasing significantly after ^{6}Li→^{7}Li replacement (Figure 7b). Meanwhile, the PVDF-HFP/LLATO interface and LiTFSI resonances showed a small ^{6}Li change, which indicated that the majority of Li ions passed through the percolated network formed by LLATO nanofibers; and only a small portion migrated via LiTFSI in the PVDF-HFP polymer matrix and along the interface. For the PVDF-HFP/LiTFSI/LLATO/Li_3PO_4 sample, in addition to the significant intensity increase of ^{6}Li signals of LLATO at -0.34 ppm and 0.12 ppm, the ^{6}Li peak of Li_3PO_4 at 0.42 ppm also increased significantly after the ^{6}Li →^{7}Li replacement (Figure 7c).

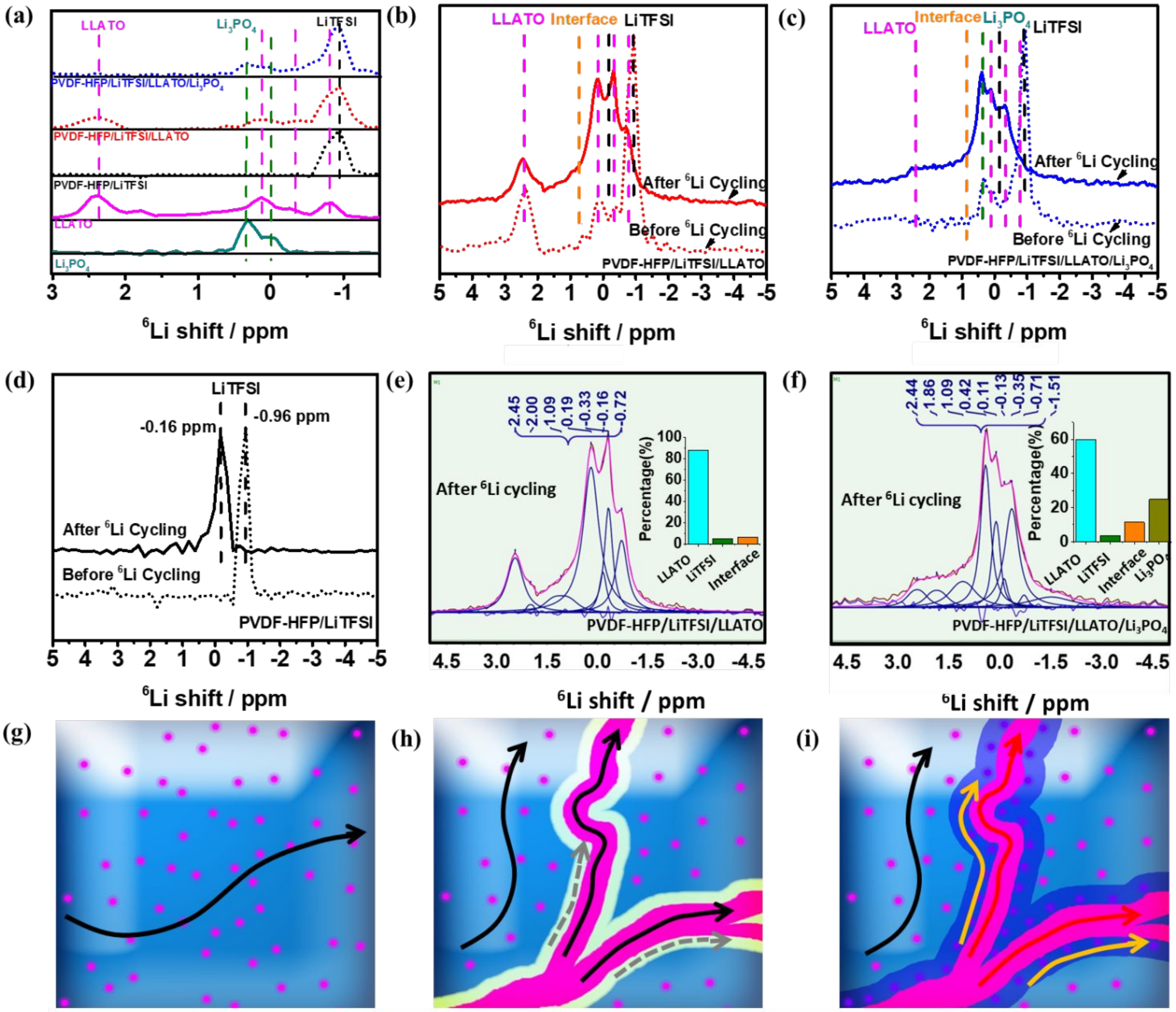

Figure. 7 Solid-state NMR spectra. (a) ^{6}Li NMR spectra of PVDF-HFP/LiTFSI, pristine LLATO, Li_3PO_4, PVDF-HFP/LiTFSI, PVDF-HFP/LiTFSI/LLATO, and PVDF-HFP/LiTFSI/LLATO/Li_3PO_4 composite electrolyte, (b) ^{6}Li NMR spectra of PVDF-HFP/LiTFSI/LLATO before and after electrochemical cycling, (c) ^{6}Li NMR spectra of PVDF-HFP/LiTFSI/LLATO/Li_3PO_4 before and after electrochemical cycling, (d) ^{6}Li NMR spectra of PVDF-HFP/LiTFSI before and after electrochemical cycling. Peak assignments and quantification results of ^{6}Li NMR signals (e) PVDF-HFP/LiTFSI/LLATO after ^{6}Li cycling, (f) PVDF-HFP/LiTFSI/LLATO/Li_3PO_4 after ^{6}Li cycling. Schematic of Li-ion pathways in (g) PVDF-HFP/LiTFSI, (h) PVDF-HFP/LiTFSI/LLATO, (i) PVDF-HFP/LiTFSI/LLATO/Li_3PO_4.

Figure 7e and 7f show the assignments and quantification results of ^{6}Li NMR signals of the PVDF-HFP/LiTFSI/LLATO and PVDF-HFP/LiTFSI/LLATO/Li_3PO_4 composite electrolytes after ^{6}Li cycling. Quantification of the ^{6}Li MAS NMR signals was calculated based on the area integrals of the simulated NMR resonances (Table S2 and Table S3). For the PVDF-HFP/LiTFSI/LLATO composite electrolyte, 87.9 mol% Li was located in the LLATO nanofibers, 5.4 mol% Li in LiTFSI, and 6.7 mol% Li in the interface. In comparison, for the PVDF-HFP/LiTFSI/LLATO/Li_3PO_4 sample, 60.0 mol% Li was in the LLATO nanofibers, 3.7 mol% Li in LiTFSI, 11.5 mol% Li in the interface, and the remaining 24.8 mol% Li is from the Li_3PO_4 buffer interface layer as shown in Table 2. The NMR analysis results suggested that lithium ions transport via three pathways: (i) intra-transport in ceramic nanofibers, (ii) intra-transport in polymer, and (ii) interfacial transport along the nanofiber/polymer interface. In addition, the interface Li signal from the PVDF-HFP/LiTFSI/LLATO/Li_3PO_4 composite was almost twice as that as the PVDF-HFP/LiTFSI/LLATO composite. The increased Li signal intensity indicated that the presence of the Li_3PO_4 layer between the LLATO nanofibers and the PVDF-HFP polymer matrix significantly improved the Li ion transport along the nanofiber/polymer interface. When a Li_3PO_4 layer was present between LLATO nanofiber and polymer, it contributed 24.8 mol% to the ^{6}Li NMR signals of the PVDF-HFP/LiTFSI/LLATO/Li_3PO_4 composite electrolytes. This additional ^{6}Li signal indicated that lithium ions transported in the Li_3PO_4 Layer. In short, the presence of Li_3PO_4 in the composite electrolyte significantly enhanced the interfacial transport along the LLTAO nanofibers/polymer interface. The ^{7}Li spectra of the composite electrolytes show the reduced intensity of the ^{7}Li resonance after ^{6}Li cycling, confirming the replacement of ^{7}Li by passing ^{6}Li ions in the LLATO phase (Figure S16).

Table 2. Li ion pathway analysis through ^{6}Li NMR: quantification results of spectral simulation.

^{6}Li signal	**PVDF-HFP/LiTFSI/LLATO (mol.%)**	**PVDF-HFP/LiTFSI/LLATO/Li_3PO_4 (mol.%)**
in LLATO nanofibers	87.9	60
in LiTFSI-polymer	5.4	3.7
at the nanofiber/polymer interface	6.7	11.5
in the interfacial Li_3PO_4 layer	--	24.8

Addition of LLATO nanofibers and Li_3PO_4 into the polymer matrix significantly improves the ionic conductivity and cyclic performance of electrolyte, which can be understood based on the analysis of three Li-ion transport pathways in the electrolyte. The LLATO nanofibers are formed a 3D network in the composite, which provides the continuous ion transport channels throughout the electrolyte. Incorporation of nanofibers with polymer leads to the amorphization of polymer, which increases the mobility of polymer chain segments, improving the Li-ion mobility in the polymer. Also, interaction of the nanofibers with the polymer results in the dehydrofluorination of PVDF chains, which weakens the electron-drawing binding energy of F, and attenuates the strong polar effect of F on the Li ions in Li-salt. This increases the mobility of lithium ions. Furthermore, the LLATO nanofiber/polymer interface is the high ionic conductivity channel for lithium ions. When more lithium ions transport along the nanofiber/polymer interface, the overall conductivity of composite electrolyte are improved. Interfacial modification with the Li_3PO_4 layer further amplifies all these effects, which further improves the ionic conductivity.

CONCLUSIONS

In summary, the LLATO nanofiber/polymer composite electrolyte exhibited much higher ionic conductivity, lithium ion transference number and better cyclic stability than monolithic polymer electrolyte. The ionic conductivity of the composite electrolyte increased with an increase in the fiber content in the composite electrolyte. The presence of a Li_3PO_4 layer between the LLATO nanofiber and the polymer further improved the ionic conductivity and cyclic stability. As a result, the ionic conductivity of the PVDF-HFP/LiTFSI/LLATO/Li_3PO_4 reached 5.1×10^{-4} S/cm. The PVDF-HFP/LiTFSI/LLATO/Li_3PO_4 exhibited a stable voltage window up to 5.0 V vs. Li|Li^+. The symmetric Li|PVDF-HFP/LiTFSI/LLATO/Li_3PO_4|Li cell showed mechanical stability during repeated lithium plating/stripping at room temperature, and a low overpotential of ~50 mV at a constant current density of 0.5 mA/cm^2. In addition, full-cell batteries assembled using this electrolyte and lithium metal anodes exhibit excellent good cycling performance and rate capability. This work shows that interfacial synergy between the ceramic nanofibers and the polymer plays important in the electrochemical performance of ceramic-polymer composite electrolytes.

There exists strong chemical interaction between the inorganic and the organic phases in the composite electrolytes. Incorporation of the LLATO nanofibers into the polymer induced dehydrofluorination of PVDF chains, deprotonation of the $-CH_2$ moiety and amorphization of the polymer matrix. Solid-state NMR spectra revealed that lithium ions transported via three pathways: the intra-polymer transport, the intra-nanofiber transport, and the interfacial polymer/nanofiber transport. The presence of Li_3PO_4 between the nanofibers and the polymer not only enhanced the chemical interaction but also greatly improved the Li ion transport along the nanofiber/polymer interface in the composite electrolyte. Fundamental understanding the interfacial ion transport and the chemical interaction at the ceramic/polymer interface will provide guidelines for design of ceramic/polymer composite electrolytes for all-solid-state lithium batteries.

EXPERIMENTAL METHODS

Chemicals and Materials. Lithium nitrate anhydrous (99.0%) and lanthanum(III) nitrate hexahydrate (99.9%), and polyvinylpyrrolidone M.W. 1,300,000 were purchased from Alfa Aesar. Titanium isopropoxide (≥99.0%), bis(trifluoromethane) sulfonimide lithium salt, (99.95% trace metals basis), poly(vinylidene fluoride-co-hexafluoropropylene) and lithium phosphate were purchased from Sigma-Aldrich. Aluminum nitrate nonahydrate (99+%) was purchased from Acros Organics. Deionized (D.I.) water was produced by a Milli-Q Millipore system (18.2 MΩ·cm, Millipore Corp., USA). All solvents were obtained from commercial sources and used without further purification.

Synthesis of $Li_{0.33}La_{0.557}TiO_3$ (LLTO) nanofibers and aluminum-doped $Li_{0.33}La_{0.557}Ti_{1-x}Al_xO_3$ (LLATO). Electrospinning precursor solutions of $Li_{0.33}La0_{.557}TiO_3$ (LLTO), Al-doped $Li_{0.33}La_{0.557}Ti_{1-x}Al_xO_3$ (LLATO) (LLATO, x=0.005; LLATO-1, x=0.01; LLATO-2, x=0.015; LLATO-3, x=0.05; LLATO-4, x=0.1) were firstly prepared. Lithium nitrate anhydrous, lanthanum(III) nitrate hexahydrate, titanium(IV) isopropoxide , and aluminum nitrate nonahydrate were used as the starting materials with a Li: La: Ti: Al ratio matching the stoichiometric molar ratio of Al-doped $Li_{0.33}La_{0.557}Ti_{1-x}Al_xO_3$. 20% excess of the lithium source was used to compensate for the lithium loss during subsequent calcination process. In a typical synthesis process for the LLATO (x=0.005), 3.96 mmol of lithium nitrate and 5.57 mmol of lanthanum(III) nitrate hexahydrate, 0.05 mmol aluminum nitrate nonahydrate were dissolved in 25 mL of de-ionized water. 9.95 mmol titanium(IV) isopropoxide was separately dissolved in a mixture of 15.27 mL of isopropanol and 5.72 mL of acetic acid. These two solutions were then mixed to create a sol. 4 g of PVP (Mw=1,300,000) was dissolved in 40 ml of DMF with 15 vol% acetic acid. The sol and PVP solution were then mixed to form the precursor solution for electrospinning. In a typical electrospinning experiment, a voltage of 19 kV was applied, the distance between the needle tip and the collector was kept constant at 15 cm, and the feed rate was 0.3 mL h^{-1}. The collector was connected to the ground.

The as-spun nanofibers were peeled off from the collector after the electrospinning, followed by calcination in an alumina combustion boat in air to remove the polymer PVP and crystallize the nanofibers.[1,2] Morphologies of the LLTO nanofibers was tuned by calcinated under different temperatures of 700 °C, 800 °C, 900 °C, and 1000 °C (Figure S1). 900°C was used for further heating treatment for LLATO nanofiber. Then LLTO nanofibers were doped with different percentage (0.5~10 mol%) of aluminum.

Lithium phosphate modification of LLATO nanofibers. Lithium phosphate was dissolved in 0.1 M phosphoric acid to form a 0.05 M solution. LLATO nanofibers were immersed in the solution for one hour. After that, the LLATO/Li_3PO_4 nanofibers were dried on a hot plate at 60 ^oC in air.

Preparation of inorganic nanofiber network-polymer composite electrolytes. A Li salt–polymer composite solution was prepared by dissolving bis(trifluoromethane)sulfonimide lithium salt (LiTFSI) and polyvinylidiene fluoride-hexafluoropropylene (PVDF-HFP) (molecular weight, ~40,000) in acetone. The composite electrolyte was prepared by dropping the Li salt-polymer solution onto the calcinated LLATO nanofiber membrane, the solvent was evaporated under air for 30 minutes. After drying, the Li salt-polymer solution wetting process was repeated. After the certain amount 70-90 wt% organic polymer was dropped onto the three-dimensional cross-linked nanofiber structure, the membrane was then kept in under vacuum before use.

Characterization. The morphologies of the samples are characterized by field-emission scanning electron microscopy (FE-SEM) and transmission electron microscopy (TEM). FESEM images were taken on JEOL JSM-7600 and Hitachi S-4700 SEMs with an accelerating voltage of 15 kV. TEM images were taken on a JEOL JEM 2100F. The crystallographic and chemical structures were characterized by an X-ray diffractometer (XRD, Rigaku DIII Ultima with Cu Kα radiation). X-ray photoelectron spectroscopy (XPS) measurements were performed on Physical Electronics PHI 5000 Versa Probe system to analyze the chemical state and atomic concentrations of elements. Binding energies (BE) were calibrated to adventitious carbon BE of 284.80 eV.

The symmetric Li|solid-state electrolyte|Li full cell was assembled in glovebox. The electrolyte membrane was sandwiched between two surface-polished lithium metal foils and sealed in 2,032 coin cells. The electrochemical stability of the electrolyte membrane was measured using linear sweep voltammetry (LSV) with a sweep rate of 1 mV/s in the range of 0–6 V. In the LSV test, the electrolyte membrane was sandwiched between stainless steel as the working electrode and lithium metal foil as the counter electrode. The ionic conductivity of the composite electrolyte was tested by electrochemical impedance spectroscopy (EIS) measurement. The electrolyte membrane was sandwiched between two stainless steel plates for the EIS measurement which was performed on a Solartron 1260 using a frequency range of 1 Hz to 1 MHz. All the samples were in a dimeter of ø=0.7 cm with a testing area of 0.385 cm^2. The pressure kept constant at 3000 psi during measurement. For measurement of the ionic conductivity, the thickness of the composite membrane were 139 μm, 111 μm, 117 μm, 115 μm, 125 μm, and 216 μm for the LLTO/PVDF-HFP/LiTFSI, LLATO/PVDF-HFP/LiTFSI, LLATO-1/PVDF-HFP/LiTFSI, LLATO-2/PVDF-HFP/LiTFSI, LLATO-3/PVDF-HFP/LiTFSI, and LLATO-4/PVDF-HFP/LiTFSI, respectively, as shown in Figure S7.

Galvanostatic cycling of the symmetric battery cells was carried out on a LANHE (CT2001A) battery testing system, with a constant current density of 0.5 mA/cm^2. For $^6Li \rightarrow ^7Li$ replacement, ^6Li metal foils were used as the two electrodes, with a constant current density of 7 $\mu A/cm^2$ biased at a potential that changed polarity every 5 min. Solid-State ^6Li NMR experiments were performed on a Bruker Avance III-500 spectrometer with a 2.5 mm Bruker HXY triple-resonance probe. The sample was spun at 25 kHz, and the spectra were collected at the ^{6}Li Larmor frequency of 73.6 MHz. LiCl with the Li shift at 0 ppm was used as a reference.

CR2032-type coin cells were assembled inside an argon-filled glovebox to evaluate the cycling performance of the composite electrolyte. The charge and discharge profiles were tested between 2.5 V to 4.2 V at different current rate at room temperature. The cells were assembled with $LiFePO_4$ cathode, Li metal anode and composite electrolyte, a trace of 2 μL carbonate electrolyte (1M $LiPF_6$ in EC: DMC: DEC=1: 1: 1 in volume ratio) was employed as a "softer contact" between the electrode and electrolyte.[42]

ASSOCIATED CONTENT

Supporting Information. Figures S1-S13. This material is available free of charge *via* the Internet at http://.

AUTHOR INFORMATION

Corresponding Author

Tel: +1-304-293-3326, E-mail: nick.wu@mail.wvu.edu

Notes

The authors declare no competing financial interest.

ACKNOWLEDGEMENTS

This material is based upon a grant by the Department of Energy (DOE), Office of Energy Efficiency and Renewable Energy (EERE) under award number DE-EE0007806. The views and opinions of the authors stated do not necessarily reflect those of the U. S. Government.

DISCLAIMER

Neither the U. S. Government, nor any of its employees, makes any warranty, express or implied, or assumes any legal liability or responsibility for the accuracy or completeness of any information, product, or process disclosed, or represents that its manufacture or use would not infringe privately owned rights. The views and opinions of the authors stated do not necessarily reflect those of the U. S. Government.

REFERENCES AND NOTES

1. H. S. Jadhav, M.-S. Cho, R. S. Kalubarme, J.-S. Lee, K.- N. Jung, K.-H. Shin, C.-J. Park, *J. Power Sources* **2013**, *241*, 502-508.
2. N. Rosenkiewitz, J. Schuhmacher, M. Bockmeyer, J. Deubener, *J. Power Sources* **2015**, *278*, 104-108.
3. S. Stramare, V. Thangadurai,a W. Weppner, *Chem. Mater.* **2003**, *15*, 3974-3990.
4. B. Wu, S. Wang, J. Lochala, D. Desrochers, B. Liu, W. Zhang, J. Yang, J. Xiao, *Energy Environ. Sci.*, **2018**, *11*, 1803-1810.
5. J. C. Bachman, S. Muy, A. Grimaud, H.H. Chang, N. Pour, S.F. Lux, O. Paschos, F. Maglia, S. Lupart, P. Lamp, and L. Giordano, *Chem. Rev.*, **2015**, *116*, 140-162.
6. P. L. Kuo, C. A. Wu, C. Y. Lu, C. H. Tsao, C. H. Hsu, S. S. Hou, *ACS Appl. Mater. Interfaces* **2014**, *6*, 3156-3162.
7. S. Liu, N. Imanishi, T. Zhang, A. Hirano, Y. Takeda, O. Yamamoto, J. Yang, *J. Electrochem. Soc.* **2010**, *157*, A1092-A1098.
8. Y. Shi, L. Peng, Y. Ding, Y. Zhao, G. Yu, *Chem. Soc. Rev.* **2015**, *44*, 6684-6696.
9. F. Croce, G.B. Appetecchi, L. Persi, B. Scrosati, *Nature* **1998**, *394*, 456–458,
10. L. R. A. K. Bandara, M. A. K. L. Dissanayake, B. E. Mellander, *Electrochimica acta*, **1998**, *43*, 1447-1451.
11. A. M. Stephan,K. S. Nahm, *Polymer* **2006**, *47*, 5952-5964.
12. W. Liu, N. Liu, J. Sun, P.C. Hsu, Y. Li, H.W. Lee, Y. Cui, *Nano Lett*, **2015**, *15*, 2740-2745.
13. X. Qian, N. Gu, Z. Cheng, X. Yang, E. Wang, S. Dong, *Electrochim. Acta* **2001**, *46*, 1829-1836.
14. J. W. Kim, K. S. Ji, J. P. Lee, J. W. Park, *J. Power Sources* **2003**, *119*, 415-421.
15.W. Wang, E. Yi, A. J. Fici, R. M. Laine, J. Kieffer, *J. Phys. Chem. C* **2017**, *121*, 2563–2573.
16. K.-S. Ji, H.-S. Moon, J.-W. Kim, J.-W. Park, *J. Power Sources* **2003**, *117*, 124–130.
17. X. Zhang, T. Liu, S. Zhang, X. Huang, B. Xu, Y. Lin, B. Xu, L. Li, C.W. Nan, Y. Shen, *J. Am. Chem. Soc.* **2017**, *139*, 13779-13785.
18. W. Liu, D. Lin, J. Sun, G. Zhou, Y. Cui, *ACS nano*, **2016**, *10*, 11407-11413.
19. P. Zhu, C. Yan, M. Dirican, J. Zhu, J. Zang, R.K. Selvan, C.C. Chung, H. Jia, Y. Li, Y. Kiyak, N. Wu, *J. Mater. Chem. A*, **2018**, *6*, 4279-4285.

20. K.K. Fu, Y. Gong, J. Dai, A. Gong, X. Han, Y. Yao, C. Wang, Y. Wang, Y. Chen, C. Yan, Y. Li, *Proc. Natl. Acad. Sci. U.S.A.* **2016**. *113*, 7094-7099.

21. X. Zhang, J. Xie, F. Shi, D. Lin, Y. Liu, W. Liu, A. Pei, Y. Gong, H. Wang, K. Liu, Y. Xiang. *Nano Lett.* **2018**, *18*, 3829−3838,

22. W. Wieczorek, Z. Florjanczyk, J. R. Stevens, *Electrochim. Acta* **1995**, *40*, 2251−2258.

23. P. Johansson, P. Jacobsson, *Solid State Ionics* **2004**, *170*, 73−78.

24. W. Liu, S.W. Lee, D. Lin, F. Shi, S. Wang, A.D. Sendek, Y. Cui, *Nature energy*, **2017**, *2*, 17035.

25. M. Wagemaker, G.J. Kearley, A.A. van Well, H. Mutka, F.M. Mulder, *J. Am. Chem. Soc.* **2003**, *125*, 840−848.

26. V. Thangadurai, W. Weppner, *Ionics*, **2000**, *6*, 70-77.

27.S. Stramare, V. Thangadurai, W. Weppner, *Chemistry of materials*, **2003**,*15*, 3974-3990.

28. P. Tarte, *J. Inorg. Nucl. Chem.*, **1967**, *29*, 915–923.

29. L. Popovic, B. Manoun, D. de Waal, M. K. Nieuwoudt, and J. D. Comins, *J. Raman Spectrosc*. **2003**, *34*, 77–83.

30. Q. Wang, C. Yang, J. Yang, K. Wu, L. Qi, H. Tang, Z. Zhang, W. Liu, H. Zhou, Energy Storage Materials, 2018, 15, 249-256.

31. *Y. Zhong, L. Zhong, S. Wang, J. Qin, D. Han, S. Ren, M. Xiao, L. Sun, and Y. Meng, Journal of Materials Chemistry A, 2019, 7, 24251-24261.*

32. S. Das, A. Ghosh, *J. Appl. Phys.* **2016**, *119*, 095101.

33. Q. Guo, Y. Han, H. Wang, S. Xiong, W. Sun, C. Zheng, K. Xie, *J. Phys. Chem. C* **2018**, *122*, 10334–10342.

34. S. Zhang, J. Shen, X. Qiu, D. Weng, W. Zhu, *J. Power Sources*, **2006**, *153*, 234–238.

35. N. A. Hashim, Y. Liu, K. Li, *Ind. Eng. Chem. Res.* **2011**, *50*, 3035–3040.

36. J. C. Daigle, A. A. Arnold, A. Vijh, K. Zaghib, *Magnetochemistry*, **2018**, *4*, 13.

37. S. Ferrari, E. Quartarone, P. Mustarelli, A. Magistris, M. Fagnoni, S. Protti, A. Spinella, *J. Power Sources*, **2010**,*195*, 559-566.

38. T. Montina, P. Wormald, P. Hazendonk, *Macromolecules*, **2012**, *45*, 6002-6007.

39. J. Zheng, M. Tang, Y.Y. Hu, *Angew. Chem. Int. Ed*, **2016**, *55*, 12538-12542.

40. J. Zheng, Y.Y. Hu, *ACS Appl. Mater. Interfaces*, **2018**, *10*, 4113-4120.

41. T. Yang, J., Zheng, Q., Cheng, Y.Y. Hu, C.K. Chan, *ACS Appl. Mater. Interfaces*, **2017**, *9*, 21773-21780

42. H. Duan, M. Fan, W.P. Chen, J.Y. Li, P.F. Wang, W.P. Wang, J.L. Shi, Y.X. Yin, L.J. Wan, Y.G. Guo, *Adv. Mater.* **2019**, *31*, 1807789.

TOC Graphic

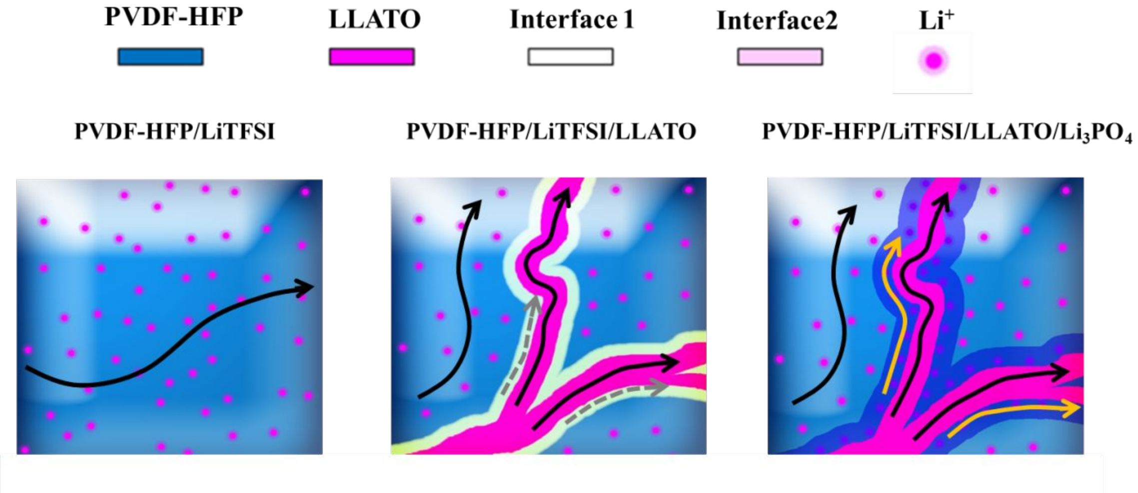
PVDF-HFP
LLATO
Interface 1
Interface2
Li$^+$
PVDF-HFP/LiTFSI
PVDF-HFP/LiTFSI/LLATO
PVDF-HFP/LiTFSI/LLATO/Li$_3$PO$_4$